

# Green Chemistry

Accepted Manuscript



This is an *Accepted Manuscript*, which has been through the Royal Society of Chemistry peer review process and has been accepted for publication.

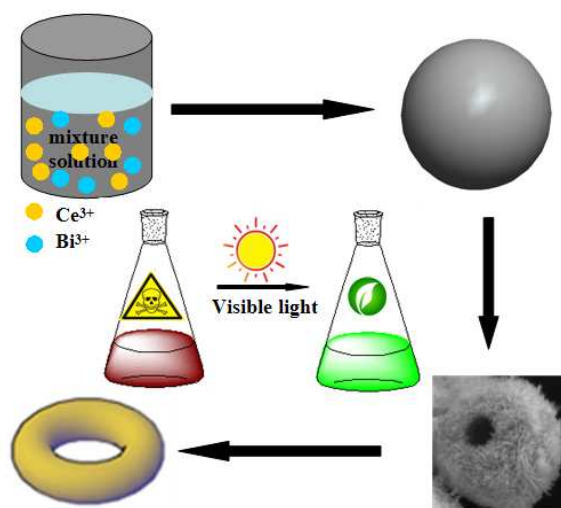
*Accepted Manuscripts* are published online shortly after acceptance, before technical editing, formatting and proof reading. Using this free service, authors can make their results available to the community, in citable form, before we publish the edited article. We will replace this *Accepted Manuscript* with the edited and formatted *Advance Article* as soon as it is available.

You can find more information about *Accepted Manuscripts* in the [Information for Authors](#).

Please note that technical editing may introduce minor changes to the text and/or graphics, which may alter content. The journal's standard [Terms & Conditions](#) and the [Ethical guidelines](#) still apply. In no event shall the Royal Society of Chemistry be held responsible for any errors or omissions in this *Accepted Manuscript* or any consequences arising from the use of any information it contains.



[www.rsc.org/greenchem](http://www.rsc.org/greenchem)

**A graphical and textual abstract for the Table of contents entry**

Ring-shaped  $\text{Bi}_2\text{WO}_6@\text{CeO}_2$  hybrid nanoparticle aggregates are fabricated through an environmental route and subsequent facile calcinations method. The intrinsic hollow ring nature as well as the p-n junction effect of the unique nanostructures contributes greatly to the enhanced performance for photocatalytic detoxification of cyanide.

## ARTICLE

## Designed hierarchical synthesis of ring-shaped $\text{Bi}_2\text{WO}_6@ \text{CeO}_2$ hybrid nanoparticle aggregates for photocatalytic detoxification of cyanide

Cite this: DOI: 10.1039/x0xx00000x

Hong Guo\*<sup>a, b</sup>, Yuanyuan Guo<sup>a</sup>, Lixiang Liu<sup>a</sup>, Tingting Li<sup>a</sup>, Wei Wang<sup>a</sup>, Weiwei Chen<sup>a</sup>, and Jing Chen<sup>a</sup>Received 00th January 2012,  
Accepted 00th January 2012

DOI: 10.1039/x0xx00000x

[www.rsc.org/](http://www.rsc.org/)

Ring-shaped  $\text{Bi}_2\text{WO}_6@ \text{CeO}_2$  hybrid nanoparticle aggregates are fabricated through an environmental route and subsequent facile calcinations method. The synthetic parameters are regulated to control the shape of the as-prepared samples. The concentration of cyanide ion decreased sharply from the initial 4.72 mM to 0.95 mM with the exposure time in 60 min. The intrinsic ring-shaped microstructure makes multiple reflections of light within the chamber, allowing more efficient use of the light source compared with solid structure. The p-n junction effect can lead to enhanced charge separation and interfacial charge transfer efficiency due to the existence of an internal electric field. Therefore, it exhibits a remarkable photocatalytic detoxification of cyanide and degradation of dye under visible light.

### Introduction

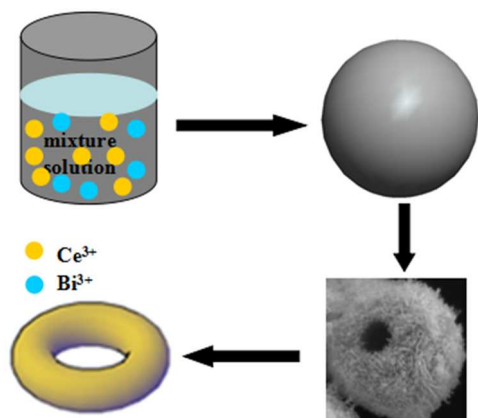
The highly toxic cyanides are present in effluent waters of several industries especially in chemical and mineral processing industry. Therefore, cyanide must be destroyed or removed from wastewater prior to discharge.<sup>1-3</sup> The normal treatment processes of cyanides are: alkaline chlorination, wet air oxidation, electrolytic oxidation, ozonation, and ion exchange, of which the alkaline chlorination is the best available proven technique.<sup>4-6</sup> However, it results in formation of highly toxic cyanogen chloride gas. Many efforts show that semiconductor photocatalysis can utilize solar energy for photocatalytic oxidation of cyanide, such as  $\text{TiO}_2$  and  $\text{ZnO}$  materials.<sup>7-11</sup> Unfortunately, the wide band gap of these materials limits its light absorption only to the UV-light range and thus most investigations are focused on photocatalytic cyanide oxidation with ultraviolet (UV) light of wavelengths of 300-400 nm, while reports on visible light photocatalytic mineralization of cyanide are quite few. The difficulty can be attributed to such reasons. The process must be stable in a highly alkaline basic medium with the value of pH ca. over 9.3 to avoid volatilization of free  $\text{CN}^-$ . The carbon in the  $\text{CN}^-$  is more strongly bound to nitrogen than with atoms in dye molecules. The adsorption of the  $\text{CN}^-$  on the photocatalytic surface becomes more difficulty with the increase of negative charge. So, photocatalytic removal of cyanide under visible light is still a great challenge. To solve these problems, designing and developing advanced hybrid micro/nano-structure materials with a heterojunction interface between two types of semiconductor with matching band potentials have attracted considerable interest in both fundamental research and practical applications due to an improvement of charge separation, an increase in the lifetime of the charge carrier, and

an enhancement of the interfacial charge transfer efficiency to adsorbed substrate.<sup>12-15</sup> For instance,  $\text{Bi}_2\text{O}_3\text{-Bi}_2\text{WO}_6$  microspheres show improved photocatalytic performance.<sup>16</sup>  $\text{Ni@SiO}_2$  nanoreactor catalysts exhibit a high temperature stability and recyclability.<sup>17</sup> Teng and co-workers obtained  $\text{Mn}_3\text{O}_4\text{-Co}_3\text{O}_4$  hollow spheres, which have a higher catalytic activity for CO oxidation than single  $\text{Co}_3\text{O}_4$  ones.<sup>18</sup> Our previous prepared yolk-shell  $\text{Ag@TiO}_2$ ,  $\text{MoO}_3\text{-SnO}_2$  and  $\text{Pd@CeO}_2$  materials exhibit enhanced catalytic, photocatalytic and energy storage properties.<sup>19-21</sup> Ce-doped  $\text{ZnO}$  nanoparticles can be used for photocatalytic detoxification of cyanide.<sup>22</sup>

Furthermore, controlling crystal phase, particle size, crystallinity, morphology of semiconductors can effectively enhance their photocatalytic performance, and thus it is another important approach to enhance the photocatalytic active. Among the common factors, morphology is regarded as one of the important factors. For example, hollow spheres, nanowires, nanotubes, and nanosheets have been proven to present better photocatalytic performance.<sup>23-27</sup> Especially, the ring structures at the nano/micro-scale are attracting fast growing interest because they can be used to find new applications owing to their specific geometry and strain-free mechanical properties resulting in structural flexibility.<sup>28-32</sup> Up to now, the common synthetic strategy for the fabrication of those structures with complex interiors employs sacrificial templates, such as polymer<sup>33</sup>, silica<sup>34</sup>, carbon inorganic spheres<sup>35</sup> and ionic liquids<sup>36</sup>. However, templating methods for constructing complex nanostructures are usually time consuming and costly because of the need for the synthesis of the templates and the multi-step templating process, and thus it is highly desirable to develop facile, scalable approaches for the rational synthesis of ring-shaped structures with designed interior structures. Therefore, a general approach to rationally fabricate ring-shaped hybrid structural nano/micro-materials for

detoxification of cyanide is still lacking and it is desirable to obtain the materials through more facile, economic and environment-friendly process. Besides, an advantage for chemists is to elaborate possible new constructions from all chemical components without any time-restricted conditions.

Herein, we chose coupled  $\text{Bi}_2\text{WO}_6@\text{CeO}_2$  to demonstrate our concept and propose a facile generic strategy to prepare ring-shaped  $\text{Bi}_2\text{WO}_6@\text{CeO}_2$  nanoparticle aggregates with a high purity, high surface areas, and enhanced photocatalytic activity on detoxification of cyanide as illustrated in Scheme 1. The alcoholysis of  $\text{Ce}^{3+}$  and  $\text{Bi}^{3+}$  leads to  $\text{Bi}_2\text{WO}_6@\text{CeO}_2$  layer with nanometer precision. At the same time, carbonization of sucrose occurs and then microspheres of carbon- $\text{Bi}_2\text{WO}_6@\text{CeO}_2$  composites will form in situ during the course of solvothermal alcoholysis, which is typically completed in 24 h. And then calcinations of the as-prepared  $\text{Bi}_2\text{WO}_6@\text{CeO}_2$  composites resulted in ring-shaped hybrid nanoparticle aggregates. Compared with conventional template-assisted methods produced  $\text{CeO}_2$ -based materials, ring-shaped  $\text{Bi}_2\text{WO}_6@\text{CeO}_2$  hybrid nanoparticle aggregates prepared as such have relatively lower density, higher surface area and more stable hollow configuration without the destructive effect of template removal on product morphology. The p-n junction effect can lead to enhanced charge separation and interfacial charge transfer efficiency due to the existence of an internal electric field. Moreover, the ring-shaped structure can make a more efficient use of the light source via multiple reflections within the interior cavity. To our best knowledge, the fabrication of ring-shaped  $\text{Bi}_2\text{WO}_6@\text{CeO}_2$  hybrid nanoparticle aggregates, which make an effective p-n junction between p-type  $\text{CeO}_2$  and n-type  $\text{Bi}_2\text{WO}_6$ , has never been reported previously. Hence, a higher degree of metal utilization as enhanced detoxification of cyanide and degradation of dye under visible light can be expected. Additionally, this route is environmentally friendly, mass-productive and low cost.



Scheme 1. Representative illustration of cage-bell  $\text{CeO}_2$  nanoparticle aggregates synthesis by solvothermal alcoholysis synthesis.

## Experimental

### Synthesis of ring-shaped $\text{Bi}_2\text{WO}_6@\text{CeO}_2$ hybrid nanoparticle aggregates

Glacial acetic acid, ethyl alcohol, sucrose,  $\text{Bi}(\text{NO}_3)_3 \cdot 6\text{H}_2\text{O}$ ,  $\text{Ce}(\text{NO}_3)_3 \cdot 5\text{H}_2\text{O}$ , and  $\text{Na}_2\text{WO}_6$  were acted as raw reagents without further purification. Water used was purified using an Ulu-pure system (Shanghai, China). In a typical procedure, sucrose (2.0 g) was dissolved in a mixture of glacial acetic

acid (18 ml), ethyl alcohol (18 ml) and water (54 ml) and stirred for 20 min.  $\text{Ce}(\text{NO}_3)_3 \cdot 5\text{H}_2\text{O}$  (1.78 g),  $\text{Bi}(\text{NO}_3)_3 \cdot 6\text{H}_2\text{O}$  (2.93 g) and  $\text{Na}_2\text{WO}_6 \cdot 2\text{H}_2\text{O}$  (1.0 g) were added to the above solution with continuous stirring to form a homogeneous solution, which was then transferred to a 200 ml Teflon-lined stainless steel autoclave. After heating in an electrical oven at 160 °C for a period of 24 h, the autoclave was cooled down naturally to room temperature. The obtained precipitate was separated by centrifuge and rinsed several times using distilled water and acetone. Finally the product was dried under vacuum at room temperature overnight. Calcinations were conducted in an electrical furnace in air at 450 °C for 4 h to remove the carbon, and then the products were obtained.

### Characterization

X-ray diffraction (XRD) was carried out to identify the phase composition of synthesized samples over the  $2\theta$  range from 20° to 90° using a Rigaku D/max-A diffractometer with Co K $\alpha$  radiation. A Fourier transform infrared spectroscope (FTIR, Thermo Nicolet 670FT-IR) was used for recording the FTIR spectra of the sample ranged from 400 to 4000  $\text{cm}^{-1}$ . Morphologies of the synthesized samples were observed with a AMRAY 1000B scanning electron microscope (SEM), and the microstructural characteristics of samples were observed by high-resolution transmission electron microscope (HR-TEM, JEOL JEM-2100) working at 200 kV accelerating voltage and the lattice structure was identified by selected area electron diffraction (SAED) technique. Nitrogen adsorption-desorption measurements were conducted at 77 K on a Micromeritics Tristar apparatus. Specific surface areas were determined following the Brunauer-Emmet-Teller analysis.

### Photocatalytic properties study

Photocatalytic activities were investigated using 300W Xe lamp with a 420 nm cutoff filter as the visible light sources. The photodegradation experiments were conducted by using a cylindrical quartz reactor with water circulation facility. For detoxification of cyanide, solutions of cyanide of the needed concentration at pH 12.5 were prepared fresh. The volume of the reaction solution was kept as 50 mL for visible light photocatalysis. Air was bubbled through the reaction solution to keep the suspended particles under continuous motion. The dissolved oxygen was determined using a luminescent optical dissolved oxygen analyzer GE-135. The cyanide ion was estimated argentometrically using p-dimethylaminobenzylidene rhodamine as the indicator. Cyanate was analyzed spectrophotometrically as previous reported. For the dye degradation experiment, photocatalytic degradation of dye were investigated by degradation of RhB and MO with an initial concentration of 10  $\text{mg} \cdot \text{L}^{-1}$  in aqueous solution. In each test, the catalyst (0.05 g) was added to 100 ml of RhB solution (10  $\text{mg} \cdot \text{L}^{-1}$ ) or 100 mL of MO solution (10  $\text{mg} \cdot \text{L}^{-1}$ ), respectively. Prior to irradiation, the suspension was magnetically stirred in the dark for 30 min to ensure the establishment of an adsorption-desorption equilibrium of the dye on the photocatalyst. Next, the solution was illuminated during 30 min. Every 5 min, 4 mL aliquots were taken and centrifuged to remove the particles. The filtrates were analyzed by UV-Vis spectrometer (400-800 nm) using Ocean Optics HR4000 high-resolution spectrometer.

## Results and discussion

### Structure and morphology of ring-shaped $\text{Bi}_2\text{WO}_6@\text{CeO}_2$ hybrid nanoparticle aggregates

The XRD patterns of the synthesized, ring-shaped  $\text{Bi}_2\text{WO}_6@\text{CeO}_2$  hybrid nanoparticle aggregates and its precursor, shown in Fig. 1a,

declare the product after calcinations at 450 °C exhibits higher crystallinity than that of precursor. The synthesized samples display composite materials corresponding to cubic fluorite-type CeO<sub>2</sub> (JCPDS card No. 81-0792) and orthorhombic Bi<sub>2</sub>WO<sub>6</sub> (JCPDS card No. 39-0256). Detailed analysis of the peak broadening of the (1 3 1) reflection using the Scherrer equation indicates an average crystallite size c.a. 8 nm, suggesting the particles are composed of nanocrystal subunits. The FTIR spectrum images of the prepared sample and that of the precursor are shown in Fig. 1b. The broad absorption peak centered at ca. 3402 is associated with the asymmetric and symmetric stretching vibrations of the -OH group of absorbed water molecules and the surface hydroxyls of the samples. For the precursor, the weak peaks from 1537 to 1391 cm<sup>-1</sup> originated from the residual carbon species. These peaks disappeared in the spectrum of synthesized final samples, indicating these organic groups have decomposed after calcinations. The strongest broad peaks in the range of 400-1100 cm<sup>-1</sup> are contributed from the metal-O<sup>37</sup>. The peak intensity is different from that of precursor, implying the structure of prepared sample has a little discrepancy with its precursor.

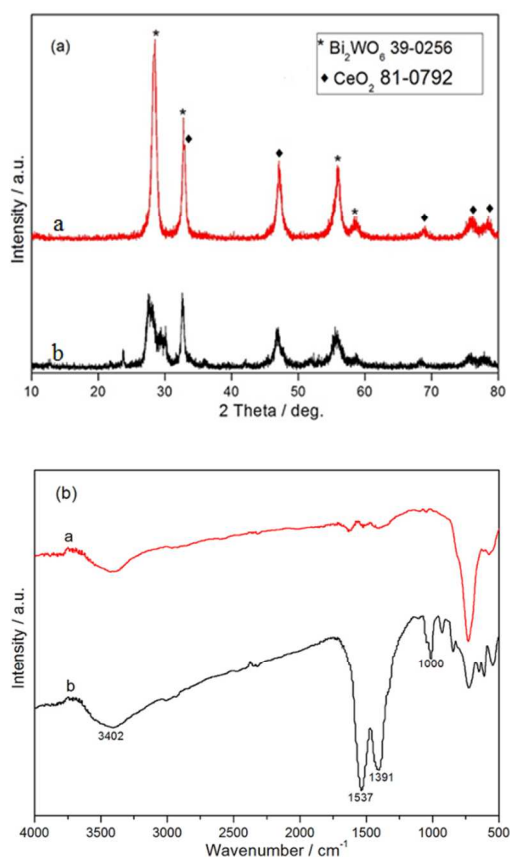


**Fig. 1** (a) XRD pattern and FTIR spectra (b) of Bi<sub>2</sub>WO<sub>6</sub>@CeO<sub>2</sub> hybrid micro-rings and its precursor corresponding to curve a and b, respectively.

SEM images of the hybrid microrings of Bi<sub>2</sub>WO<sub>6</sub>@CeO<sub>2</sub> yielded by calcinations at 450 °C are shown as Fig. 2a and b. Fig. 2a illuminates the as-synthesized samples are uniform ring shape, with an average size of ca. 2 μm. It can be clearly noticed that the obtained Bi<sub>2</sub>WO<sub>6</sub>@CeO<sub>2</sub> powder is not a solid ball but a hollow loose microstructure characteristic according to Fig. 2b, and it is interesting to find that the microring is made up from nanosheets. The unique ring morphology of Bi<sub>2</sub>WO<sub>6</sub>@CeO<sub>2</sub> hybrid nanoparticle

aggregates is also characterized by TEM and HR-TEM, as illustrated in Fig. 2c-e. Fig. 2c shows the resulting Bi<sub>2</sub>WO<sub>6</sub>@CeO<sub>2</sub> mesospheres are visible hollow ring shape obviously, which is consistent with the SEM analysis. This structure is almost the same as the expected model shown in Scheme 1. Fig. 2d confirms that the relatively large microring is aggregates of thin nanosheets. Moreover, orthorhombic Bi<sub>2</sub>WO<sub>6</sub> nanoparticles with a size of 5–8 nm are found to be doped in the nanosheet according to the HRTEM image (Fig. 2e). The detected lattice spacing (0.236 nm) agrees with Bi<sub>2</sub>WO<sub>6</sub> (1 1 1) plane spacing. The selected area electron diffraction (SAED) pattern is displayed in Fig. 2f, which clearly reveal the presence of cubic fluorite-type CeO<sub>2</sub> and orthorhombic Bi<sub>2</sub>WO<sub>6</sub>. The (2 2 0) and (3 1 1) planes of cubic CeO<sub>2</sub>, and (1 3 1) and (2 0 0) planes of orthorhombic Bi<sub>2</sub>WO<sub>6</sub> are seen through their interplanar spacing. These results are in total agreement with the observed XRD analysis. The unique p-n ring-shaped Bi<sub>2</sub>WO<sub>6</sub>@CeO<sub>2</sub> hybrid structure is expected to be favorable for enhanced catalytic activity for detoxification of cyanide.

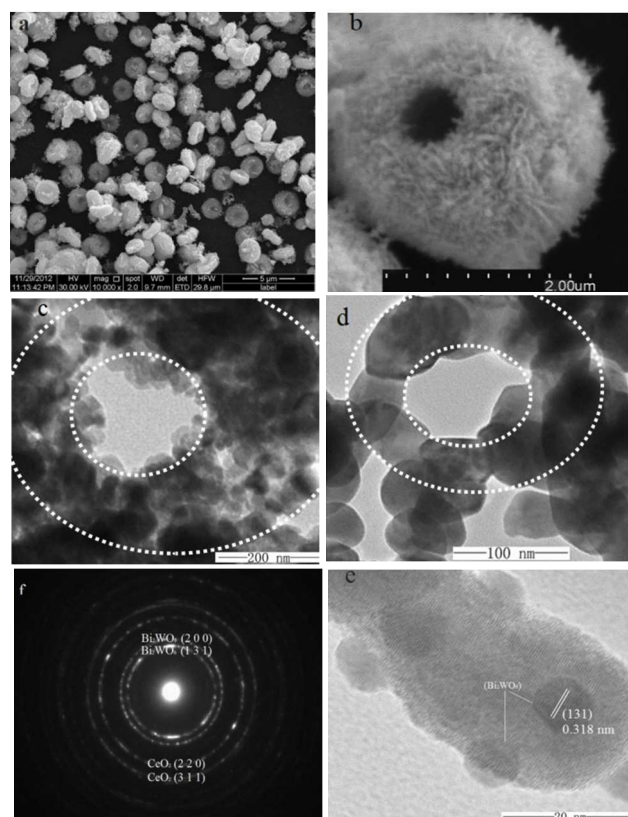


**Fig. 2** SEM (a, b), TEM (c, d) images, HRTEM micrographs (e), and selected area electron diffraction (f) of as-synthesized Bi<sub>2</sub>WO<sub>6</sub>@CeO<sub>2</sub> hybrid microrings, which is yielded by solvothermal alcoholysis at 160 °C for 24 h in 90 ml mixed solvent with proportion of 1 : 1 : 3 (V%) of glacial acetic acid, ethyl alcohol and water, and subsequent calcinations in air at 450 °C.

The N<sub>2</sub> adsorption/desorption isotherms and the pore size distribution of the obtained Bi<sub>2</sub>WO<sub>6</sub>@CeO<sub>2</sub> hybrid micro-rings is shown as Fig. 3a. The isotherm is identified as type IV, which is the characteristic isotherm of mesoporous materials. The BET surface area of the sample is 92.35 m<sup>2</sup>g<sup>-1</sup>. The room temperature UV-vis absorption spectrum of the resulting sample is shown in Fig. 3b, which exhibits a wide visible-light absorption in the range of 400–700 nm.

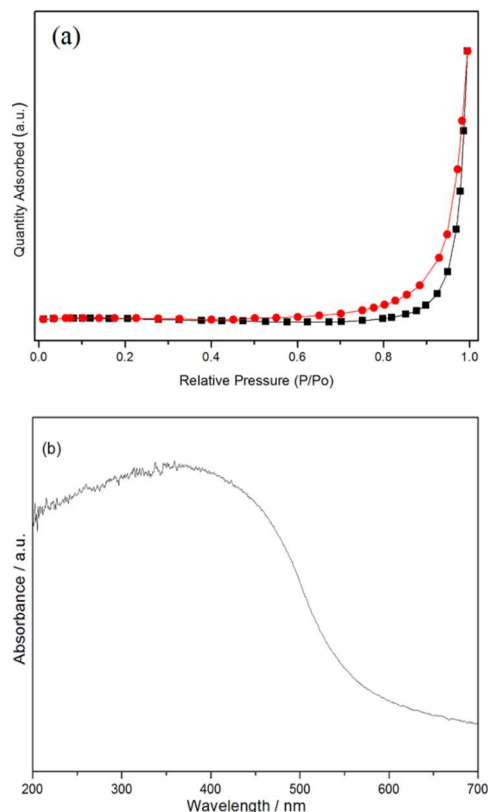


**Fig. 3** Nitrogen adsorption/desorption isotherm (a) and UV-Vis diffuse reflectance spectrum (b) of  $\text{Bi}_2\text{WO}_6\text{-CeO}_2$  hybrid micro-rings.

#### Synthesis of cage-bell $\text{Bi}_2\text{WO}_6\text{@CeO}_2$ hybrid micro-rings with controlled morphologies

The formation mechanism is tracked to investigate according to Fig.4, which are SEM images of solvothermal reaction for 24 h at  $160^\circ\text{C}$  for mixed solvent with different proportions of glacial acetic acid (GAA), ethyl alcohol (EA), and water (W) after calcination at  $450^\circ\text{C}$  for 4 h. In solvothermal alcoholysis-hydrolysis process, accompanying the simultaneous reactions (hydrolysis of  $\text{Bi}^{3+}$  and  $\text{Ce}^{3+}$ , and carbonization of sucrose) occurring, Ostwald ripening process is promoted by the little water added in the solvothermal process. To confirm the component of the resulting carbon/ $\text{Bi}_2\text{WO}_6\text{@CeO}_2$  hybrid micro-rings composite in deeply, composites of  $\text{HNO}_3$  and  $\text{H}_2\text{O}_2$  were hired to remove the  $\text{Bi}_2\text{WO}_6\text{@CeO}_2$  and gave rise to carbon according to XRD (Fig. S1<sup>†</sup>) and SEM (Fig. S2<sup>†</sup>), which confirms the amorphous carbon is well-proportioned loaded with  $\text{Bi}_2\text{WO}_6\text{@CeO}_2$  nanoparticles. So the ring structure nanoparticle forms uniformly. Based on such analysis, hydrolysis of  $\text{Bi}^{3+}$  and  $\text{Ce}^{3+}$  and carbonization of organics occurred at the same time. It is found that only solid  $\text{Bi}_2\text{WO}_6\text{@CeO}_2$  nano aggregates exist in solvent systems (GAA: EA: W = 1: 1: 0, Fig. 4a), which is considered as no water exist, so the rate of hydrolysis of  $\text{Bi}^{3+}$  and  $\text{Ce}^{3+}$  is not as fast as that of carbonization of sucrose, and thus the produced amorphous carbon is not loaded but surrounded on the  $\text{Bi}_2\text{WO}_6\text{@CeO}_2$  nanoparticles. Therefore, the product is solid structure after calcinations. When the  $\text{H}_2\text{O}$  content in the mixed solvent is increased, the rate of hydrolysis of  $\text{Bi}^{3+}$  and  $\text{Ce}^{3+}$  quickens and part hydrolysis products load on the produced amorphous carbon template and grow vigorously. Consequently, the surface of sample changes coarsely as Fig. 4b and c. Further enhanced the content of water, the interior of the sphere changed empty gradually such as Fig.

4d (GAA: EA: W = 1: 1: 2.5) and 4e (GAA: EA: W = 1: 1: 4). Finally, the hollow ring structure is broken wholly and shows flower-like morphology (Fig. 4f, GAA: EA: W = 1: 1: 8). According to above experiments, it can be speculated that the formation of the hollow ring-shaped  $\text{Bi}_2\text{WO}_6\text{@CeO}_2$  hybrid nanoparticle aggregates goes through the formation of solid core and the transformation of the solid spheres coarse surface to hollow ring-shaped ones is based on the Ostwald ripening process.

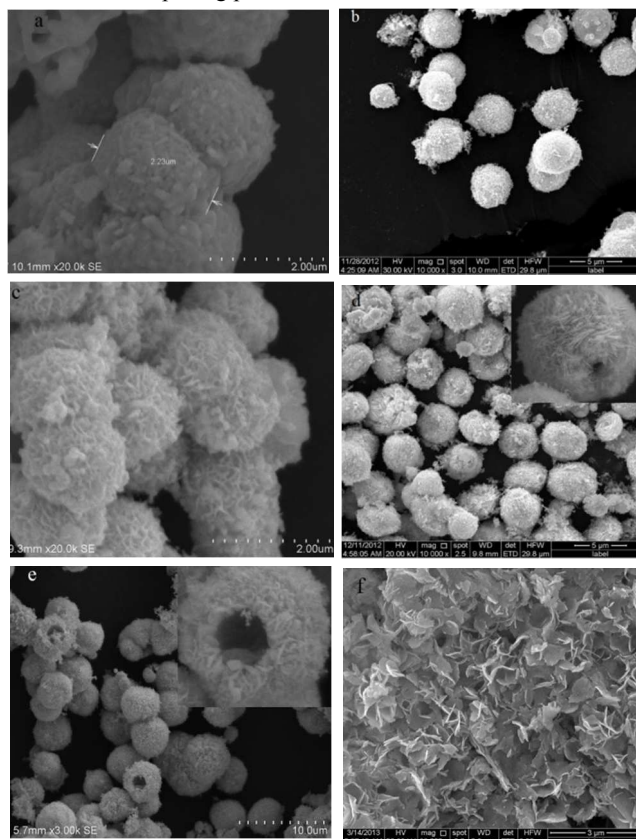


**Fig. 4** SEM images of solvothermal reaction at  $160^\circ\text{C}$  for mixed solvent (90 ml) with different proportions (V%) of glacial acetic acid (GAA), ethyl alcohol (EA), and water (W) after calcination at  $450^\circ\text{C}$  for 4 h. (a) GAA: EA: W = 1: 1: 0, (b) GAA: EA: W = 1: 1: 0.5, (c) GAA: EA: W = 1: 1: 1, (d) GAA: EA: W = 1: 1: 2, (e) GAA: EA: W = 1: 1: 2.5, (f) GAA: EA: W = 1: 1: 4, (f) GAA: EA: W = 1: 1: 8.

#### Catalytic activity

##### Photocatalytic detoxification of cyanide.

Cyanide ion is not degraded under illumination in the absence of photocatalyst, nor in the dark in the presence of the photocatalyst. The time profiles of cyanide oxidation catalyzed by  $\text{Bi}_2\text{WO}_6\text{@CeO}_2$  hybrid materials under visible light are shown as Fig.5a, implying a steady and continuous degradation of the cyanide ion. The concentration of cyanide ion decreased sharply from the initial 4.72 mM to 0.95 mM with the exposure time in 60 min. However, the commercial  $\text{CeO}_2$  and  $\text{Bi}_2\text{WO}_6$  have not significant effect. The large surface area renders the  $\text{Bi}_2\text{WO}_6\text{@CeO}_2$  hybrid materials a high activity. The ring-shaped structure of  $\text{Bi}_2\text{WO}_6\text{@CeO}_2$  hybrid materials makes multiple reflections of light within the chamber, allowing more efficient use of the light source. Moreover, the p-n junction effect can lead to enhanced charge separation and interfacial charge transfer efficiency. All the factors contribute greatly to the improved visible light catalytic activity. Compared with the other

reports<sup>7-11, 25, 38, 39</sup>, our strategy provides a novel route to prepare ring-shaped hybrid materials with higher efficiency for photocatalytic detoxification of cyanide.

### Photocatalytic degradation of dye

Photocatalytic activity is also investigated by degradation of MO and RhB, and photodecomposition results are shown in Fig. 5b and c. The difference of spectrum between the original solution and after stirred in the dark for 20 min should be attributed to adsorption-desorption equilibrium between the photocatalyst and organic dyes. It can be noted a continual fading of the coloration of both RhB and MO solutions as a function of reaction time in the presence of the samples, implying a steady and continuous degradation of the organic dyes. Fig. 3b reveals a gradual decrease of MO aqueous absorption at the wavelength of 464 nm. Surprisingly, the color of the supernatant changes from yellow to colorless observed by the naked eye after visible light irradiation for 25 min. The concentration of MO decreased sharply with the exposure time, and over 97.5% of MO is degraded within 30 min, showing significant efficiency in the photodecomposition of MO. The main absorption peak of RhB completely disappears after 25 min irradiation according to Fig. 5c. The photocatalytic conversion of RhB degradation is up to 99.8% after 30 min of irradiation. At last, no new absorption bands are found in both the ultraviolet and visible regions, indicating the complete photodegradation of RhB. Compared with most reported  $\text{Bi}_2\text{WO}_6$ <sup>40-43</sup> and  $\text{CeO}_2$ <sup>44-47</sup> based composites used for photocatalytic activity MO and RhB under visible light, our prepared ring-shaped  $\text{Bi}_2\text{WO}_6@/\text{CeO}_2$  hybrid nanoparticle aggregates exhibit higher photocatalytic activity.

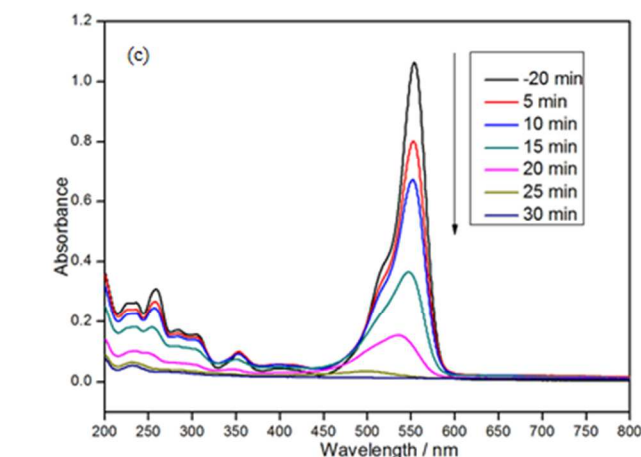
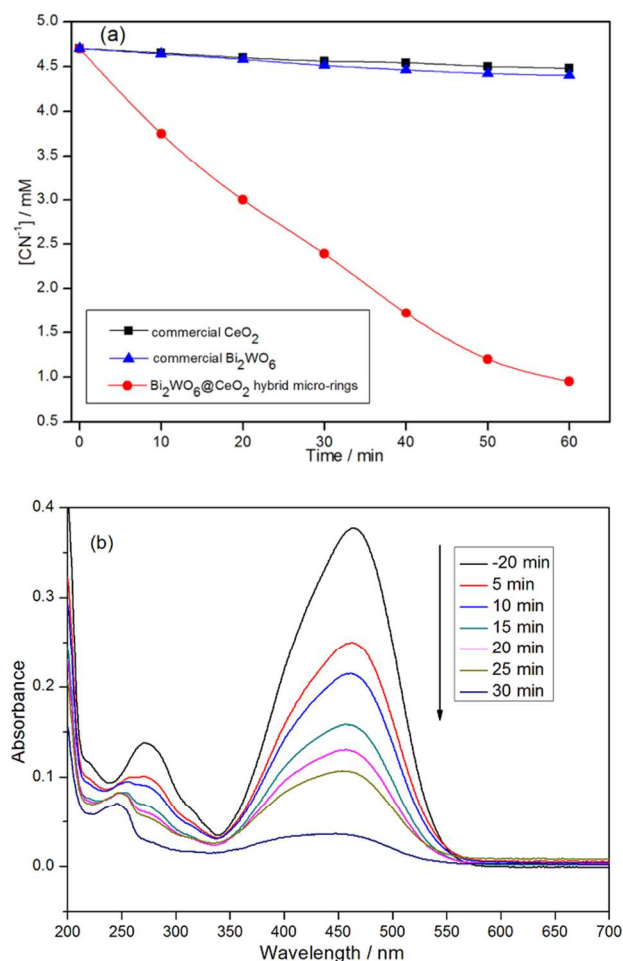


Fig. 5 Photodecomposition results: (a) comparison of detoxification of cyanide in the presence of commercial  $\text{Bi}_2\text{WO}_6$  and  $\text{CeO}_2$ , pH = 12.5, catalyst loading = 0.02 g, airflow rate =  $8.5 \text{ mL s}^{-1}$ ,  $[\text{O}_2]_{\text{dissolved}} = 28.8 \text{ ppm}$ . The absorption spectrum of dissolved MO (b) and RhB (c) in the presence of  $\text{Bi}_2\text{WO}_6@/\text{CeO}_2$  samples (0.05 g).

### Conclusions

Ring-shaped structure of  $\text{Bi}_2\text{WO}_6@/\text{CeO}_2$  hybrid nanoparticle aggregates are successfully synthesized by a facile and environmentally benign procedure combining with solvothermal alcoholysis synthesis and subsequent calcinations. It exhibits a remarkable activity for photocatalytic detoxification of cyanide and degradation of dye. This strategy is simple, cheap and mass-productive, which may shed light on a new avenue for large-scale synthesis of ring-shaped structural nano/micro functional hybrid materials for catalyst, energy and other applications.

### Acknowledgements

The authors would like to acknowledge financial support provided by Department Science Foundation of China (No.210204), National Natural Science Foundation of China (No.U0937601), 863 Program of National High Technology Research Development Project of China (No. 2011AA03A405) and Major state basic research development program of China (973 Program, No. 2014CB643406).

### Notes and references

<sup>a</sup> School of Chemistry Science and Engineering, Yunnan University, Kunming 650091, Yunnan, China. Fax: +86-871-65036626; Tel: +86-871-65032180; E-mail: guohongcom@126.com

<sup>b</sup> School of Chemistry Science and Engineering, Qujing Normal University, Qujing 65500, Yunnan, China

Electronic Supplementary Information (ESI) available: [details of any supplementary information available should be included here]. See DOI: 10.1039/b000000x/

- 1 R.R. Dash, C. Balomajumder and A. Kumar, *J. Chem. Eng.*, 2009, **146** 408.
- 2 J. Ma and P.K. Dasgupta, *Anal. Chim. Acta*, 2010, **673**, 117.
- 3 J.N. Smith, A. Keil, J. Likens and R.G. NollCooks, *Analyst*, 2010, **135**, 994.
- 4 R.R. Dash, A. Gaur and G. J. *Hazard. Mater.*, 2009, **163**, 1.
- 5 R. C. Rocha-e-Silva, L. A. V. Cordeiro and B. Soto-Blanco, *Comp. Biochem. Phys. C*, 2010, **151**, 294.
- 6 M. Banea, G. Nahimana, C. Mandombi, J. H. Bradbury, I. C. Denton and N. Kuwa, *Food Chem. Toxicol.*, 2012, **50**, 1517.

- 7 J. Marugan, R.V. Grieken, A.E. Cassano and O.M. Alfano, *Catal. Today*, 2009, **144**, 87.
- 8 J. Marugan, R.V. Grieken, A.E. Cassano and O.M. Alfano, *Appl. Catal. B*, 2008, **85**, 48.
- 9 H. Guo, D. Tian, L. Liu, Y. Wang, Y. Guo and X. Yang, *J. Solid State Chem.*, 2013, **201**, 137.
- 10 A. Bozzi, I. Guasaquillo and J. Kiwi, *Appl. Catal. B*, 2004, **51**, 203.
- 11 M. Shang, W. Wang, Z., L. Zhang, S.M. Sun, L. Wang and L. Zhou, *J. Phys. Chem. C*, 2009, **113**, 14727.
- 12 L.S. Zhang, K.H. Wong, Z.G. Chen, J. C.Yu, J. C. Zhao, C. Hu, C. Y.Chan and P. K. Wong, *Appl. Catal., A*, 2009, **363**, 221.
- 13 M. C. Long, W. M. Cai, J. Cai, B. X. Zhou, X. Y. Chai and Y. H. Wu, *J. Phys. Chem. B*, 2006, **110**, 820211.
- 14 S. Y. Chai, Y. J. Kim, M. H. Jung, A. K. Chakraborty, D. Jung and W. I. Lee, *J. Catal.*, 2009, **262**, 144.
- 15 Y. Bessekhoud, D. Robert and J.-V. Weber, *J. Photochem. Photobiol. A*, 2004, **163**, 569.
- 16 M. Ge, Y. Li, L.Liu, Z. Zhou and W. Chen, *J. Phys. Chem. C*, 2011, **115**, 5220.
- 17 J. C. Park, J. U. Bang, J. Lee, C. H. Ko and H. Song, *J. Mater. Chem.*, 2010, **20**, 1239.
- 18 F. Teng, T. Xu, S. Liang, G. Buerger, W. Yao and Y. Zhu, *Catal. Commun.*, 2008, **9**, 1119.
- 19 H. Guo, W. Wang, L. Liu, Y. He, C. Li and Y. Wang, *Green Chem.*, 2013, **15**, 2810.
- 20 H. Guo, Y. He, Y. Wang, L. Liu, X. Yang, S. Wang, Z. Huang and Q. Wei, *J. Mater. Chem. A*, 2013, **1**, 7494.
- 21 H. Guo, L. Liu, Ti. Li, W. Chen, Y. Wang and W. Wang, *Chem. Commun.*, 2014, **50**, 673.
- 22 C. Karunakaran, P. Gomathisankar and G. Manikandan, *Mater. Chem. Phys.*, 2010, **123**, 585.
- 23 Z. F. Bian, J. Zhu, J. G. Wang, S. X. Xiao, C. Nuckolls and H. X. Li, *J. Am. Chem. Soc.*, 2012, **134**, 2325.
- 24 D. J. Xue, S. Xin, Y. Yan, K. C. Jiang, Y. X. Yin, Y. G. Guo and L. J. Wan, *J. Am. Chem. Soc.*, 2012, **134**, 2512.
- 25 C. Karunakaran and P. Gomathisankar, *ACS Sustainable Chem. Eng.* 2013, dx.doi.org/10.1021/sc400195n .
- 26 D. Sarkar, C. K. Ghosh, S. Mukherjee and K. K. Chattopadhyay, *ACS Appl. Mater. Inter.*, 2013, **5**, 331.
- 27 H. Gnayem and Y. Sasson, *ACS Catal.*, 2013, **3**, 186.
- 28 X. Y. Kong, Y. Ding, R. Yang and Z. L. Wang, *Science*, 2004, **303**, 1348.
- 29 J. Wu, Z. M. Wang, V. G. Dorogan, S. Li, J. Lee, Y. I. Mazur, E. S. Kim and G. J. Salamo, *Nanoscale Res. Lett.*, 2013, **8**, 5.
- 30 C. J. Jia, L. D. Sun, F. Luo, X. D. Han, L. J. Heyderman, Z. G. Yan, C. H. Yan, K. Zheng, Z. Zhang and M. Takano, *J. Am. Chem. Soc.*, 2008, **130**, 16968.
- 31 X. Li, *J. Phys. Chem. C*, 2010, **114**, 15343.
- 32 Q. Sun, Q. Wang, P. Jena, J. Yu and Y. Kawazoe, *Phys. Rev. B: Condens. Matter Mater. Phys.*, 2004, **70**, 2454.
- 33 X. Lai, J. Li, B. A. Korgel, Z. Dong, Z. Li, F. Su, J. Du and D. Wang, *Angew. Chem. Int. Ed.*, 2011, **50**, 2738.
- 34 D. Wang and H. Zeng, *Chem. Mater.* 2009, **21**, 4811.
- 35 H. Guo, Y. P. Wang, W. Wang, L. X. Liu, Y. Y. Guo, X. J. Yang and S. X. Wang, *Part. Part. Syst. Charact.*, 2013, DOI: 10.1002/ppsc.201300198.
- 36 T. Nakashima and N. Kimizuka, *J. Am. Chem. Soc.*, 2003, **125**, 6386.
- 37 P. R. Griffiths, D.J.A. Haseth, *Fourier Transform Infrared Spectrometry*, John Wiley & Sons, New York, 1986.
- 38 C. Karunakaran, G. Abiramasundari, P. Gomathisankar, G. Manikandan and V. Ananthi, *Mater. Res. Bull.*, 2011, **46**, 1586.
- 39 J. R. Parga, V. Vázquez, H. M. Casillas and J. L. Valenzuela, *Chem. Eng. Technol.*, 2009, **32**, 1901.
- 40 X.J. Dai, Y.S. Luo, W.D. Zhang and S.Y. Fu, *Dalton Trans.*, 2010, **39**, 3426.
- 41 M. Guan, D. Ma and S. Hu, *Inorg. Chem.*, 2011, **50**, 800.
- 42 M. Ge, Y. Li, L. Liu, Z. Zhou and W. Chen, *J. Phys. Chem. C*, 2011, **115**, 5220.
- 43 X. Li, R. Huang and Y. Hu, *Inorg. Chem.*, 2012, **51**, 6245.
- 44 S. Hu, F. Zhou, L. Wang and J. Zhang, *Catal. Commun.*, 2011, **12**, 794.
- 45 C. Zhang and J. Lin, *Phys. Chem. Chem. Phys.*, 2011, **13**, 3896.
- 46 N. S. Arul, D. Mangalaraj, P. C. Chen, N. Ponpandian, P. Meena and Y. Masuda, *J. Sol-Gel Sci. Technol.*, 2012, **64**, 515.
- 47 L. Huang, Y. Li, H. Xu, Y. Xu, J. Xia, K. Wang, H. Lia and X. Cheng, *RSC Adv.*, 2013, DOI: 10.1039/c3ra42712a.